Acta Pharmacologica Sinica

ARTICLE

Crosstalk between the Akt/mTORC1 and NF-κB signaling pathways promotes hypoxia-induced pulmonary hypertension by increasing DPP4 expression in PASMCs

Ying Li[1,2], Li Yang[3], Liang Dong[1], Zhi-wei Yang[4], Jing Zhang[1], Sheng-li Zhang[4], Meng-jie Niu[5], Jing-wen Xia[1], Yi Gong[1], Ning Zhu[1], Xiu-juan Zhang[1], Yuan-yuan Zhang[1], Xiao-min Wei[1], You-zhi Zhang[1], Peng Zhang[1] and Sheng-qing Li[1]

Abnormal wound healing by pulmonary artery smooth muscle cells (PASMCs) promotes vascular remodeling in hypoxia-induced pulmonary hypertension (HPH). Increasing evidence shows that both the mammalian target of rapamycin complex 1 (mTORC1) and nuclear factor-kappa B (NF-κB) are involved in the development of HPH. In this study, we explored the crosstalk between mTORC1 and NF-κB in PASMCs cultured under hypoxic condition and in a rat model of hypoxia-induced pulmonary hypertension (HPH). We showed that hypoxia promoted wound healing of PASMCs, which was dose-dependently blocked by the mTORC1 inhibitor rapamycin (5−20 nM). In PASMCs, hypoxia activated mTORC1, which in turn promoted the phosphorylation of NF-κB. Molecular docking revealed that mTOR interacted with IκB kinases (IKKs) and that was validated by immunoprecipitation. In vitro kinase assays and mass spectrometry demonstrated that mTOR phosphorylated IKKα and IKKβ separately. Inhibition of mTORC1 decreased the level of phosphorylated IKKα/β, thus reducing the phosphorylation and transcriptional activity of NF-κB. Bioinformatics study revealed that dipeptidyl peptidase-4 (DPP4) was a target gene of NF-κB; DPP4 inhibitor, sitagliptin (10−500 μM) effectively inhibited the abnormal wound healing of PASMCs under hypoxic condition. In the rat model of HPH, we showed that NF-κB activation (at 3 weeks) was preceded by mTOR signaling activation (after 1 or 2 weeks) in lungs, and administration of sitagliptin (1−5 mg/kg every day, ig) produced preventive effects against the development of HPH. In conclusion, hypoxia activates the crosstalk between mTORC1 and NF-κB, and increased DPP4 expression in PASMCs that leads to vascular remodeling. Sitagliptin, a DPP4 inhibitor, exerts preventive effect against HPH.

Keywords: pulmonary hypertension; mTORC1; NF-κB; IκB kinase; DPP4; sitagliptin; pulmonary artery smooth muscle cells

Acta Pharmacologica Sinica (2019) 40:1322–1333; https://doi.org/10.1038/s41401-019-0272-2

INTRODUCTION

Hypoxia-induced pulmonary hypertension (HPH) comprises a heterogeneous group of diseases characterized by chronic hypoxia, including altitude sickness and chronic pulmonary diseases, in which vascular inflammation and abnormal responses to vascular injury initiate pulmonary vascular remodeling [1, 2]. Pulmonary artery smooth muscle cells (PASMCs) contribute to obliterative vascular remodeling and have enhanced proliferation, suppressed apoptosis, and increased migratory potential [3]. Hyperactivation of the Akt/mammalian target of rapamycin (mTOR) pathway increases the proliferation and survival of PASMCs and promotes the development of HPH [4]; mTORC1 inhibitor rapamycin reduced pulmonary vascular remodeling by inhibiting cell proliferation via Akt/mTOR signaling pathway downregulation in several pulmonary hypertension rat models [5–7]. However, the side effects of rapamycin, including toxicity, carcinogenicity, delayed healing and immunosuppressive effects, limit its long-term use in patients with pulmonary hypertension [8, 9].

Inflammation contributes to the pathogenesis of various forms of pulmonary hypertension. The expression of NF-κB is increased in the lung tissue of a rat model of HPH, and NF-κB activation may contribute to the development of this condition [10]. Inhibition of NF-κB by pyrrolidine dithiocarbamate has a therapeutic effect on severe HPH [11]. Ruscogenin has been reported to have beneficial effects on monocrotaline-induced pulmonary hypertension by inhibiting NF-κB expression [12]. NF-κB is also activated in the pulmonary vessels of patients with end-stage idiopathic pulmonary arterial hypertension [13]. These findings highlight the key role of NF-κB in the abnormal response to vascular injury in HPH.

In this study, we found that mTOR phosphorylation was followed by NF-κB activation in a rat model of HPH. We hypothesized that investigating the crosstalk between the mTOR and NF-κB signaling pathways may aid in understanding the molecular mechanism underlying the hypoxia-induced abnormal response to vascular injury. Moreover, investigation of NF-κB and

[1]Department of Pulmonary and Critical Care Medicine, Huashan Hospital, Fudan University, Shanghai 200040, China; [2]Department of Respiratory Medicine, Shaanxi Provincial Second People's Hospital, Xi'an 710005, China; [3]Department of Anesthesiology, Grade 2014, Chongqing Medical University, Chongqing 400016, China; [4]Department of Applied Physics, Xi'an Jiaotong University, Xi'an 710049, China and [5]Department of Gastroenterology Medicine, Xi'an Third Hospital, Xi'an 710018, China
Correspondence: Sheng-qing Li (shengqingli@hotmail.com)
These authors contributed equally: Ying Li, Li Yang, Liang Dong, Zhi-wei Yang, Jing Zhang

Received: 1 February 2019 Revised: 10 June 2019 Accepted: 11 June 2019
Published online: 17 July 2019

its downstream target proteins may help to identify new target proteins for drug development in HPH.

MATERIALS AND METHODS

A rat model of HPH

Adult male Sprague-Dawley rats weighing 150–200 g were purchased from the Laboratory Animal Center, Fourth Military Medical University (Xi'an, China). All protocols and surgical procedures were approved by the Fourth Military Medical University Veterinary Medicine Animal Care and Use Committee.

Animals were divided randomly into the following five groups ($n = 8$/group): (1) normoxia, (2) chronic hypoxia, (3) chronic hypoxia and treatment with 1 mg/kg per day sitagliptin, (4) chronic hypoxia and treatment with 2 mg/kg per day sitagliptin, and (5) chronic hypoxia and treatment with 5 mg/kg per day sitagliptin. Sitagliptin was administered via gavage. Rats in the normoxia group were housed at ambient barometric pressure for 28 days (~718 mmHg, PO_2 was ~150.6 mmHg). Rats in the hypoxia groups were housed in a hypobaric hypoxia chamber depressurized to 380 mmHg (PO_2 was reduced to ~79.6 mmHg) for 8 h/day for 28 days. All animals were housed under a 12:12 h light–dark cycle and had free access to food and water. The room temperature was maintained at 25 °C, and the bedding was changed once per week.

Hemodynamic analysis and tissue preparation

After exposure to hypoxia for 28 days, the rats were fasted overnight and anesthetized with 20% ethyl urethane (4 mL/kg i.p.). Next, the right jugular vein was carefully isolated, and a specially shaped catheter linked to a PowerLab system (AD Instruments, Bella Vista, NSW, Australia) was inserted into the right ventricle (RV) via this vein; then, the right ventricular systolic pressure (RVP) was recorded. Next, a sternotomy was performed, and the rats were perfused with paraformaldehyde. Both lungs and the heart were harvested. The RV and the left ventricle plus septum (LV+S) were weighed, and the RV/LV+S weight ratio was determined to be an indication of right ventricular hypertrophy. Next, the lower lobe of the right lung was sectioned into 4-mm-thick slices and soaked in a 10% formalin solution (pH = 7.4). The other tissues were kept at −80 °C for further experiments.

Hematoxylin and eosin (H&E) staining

The fixed lungs were sliced along the mid-sagittal plane, embedded in paraffin, and cut into ~5-μm-thick sections with a microtome. Then, the sections were placed on glass slides, stained with hematoxylin and eosin (H&E) for morphological analysis, and visualized under an Olympus BX41 microscope (Tokyo, Japan).

Culture and transfection of primary rat PASMCs

Fresh human pulmonary small artery samples were obtained from patients undergoing lung transplantation diagnosed with advanced stage chronic obstructive pulmonary disease (COPD) and pulmonary hypertension (PH). These patients are usually classified as group III PH. Human and rat PASMCs were obtained via an explant method as described previously [14]. Smooth muscle cells were grown in Dulbecco's modified Eagle's medium (DMEM) supplemented with 20% (*v*/*v*) fetal bovine serum and verified by staining for smooth muscle α-actin at each passage (>95% of cells were positively stained). Cells were used at passages 3–6. In the response to the vascular injury assay, PASMCs were exposed to normoxia, hypoxia, and hypoxia plus various inhibitors as indicated. Cells in the normoxia group were maintained at 37 °C in 21% O_2 and 5% CO_2 (HH·CP-01W, Shanghai Boxun Industry & Commerce Co., Ltd., Shanghai, China). Cells in the hypoxia groups were separately cultured in 1% oxygen, 94% N_2, and 5% CO_2 for 48 h (HERAcell 240, Heraeus Inc., Kendro, Germany).

When primary cultured PASMCs reached 80% confluency, they were transfected with the Flag-NF-κB (p65) plasmid using X-tremeGENE HP DNA Transfection Reagent (Roche Company, Mannheim, Germany) according to the manufacturer's protocol and cultured for 24 h.

Lentiviral infection

The lentiviral expression vectors, including Gipz-shmTOR/Raptor/NF-κB, and packaging vectors, including pMD2.0 G and psPAX, were purchased from Addgene (Cambridge, MA, USA). To prepare mTOR/Raptor/NF-κB viral particles, HEK293T cells were transfected with each viral vector and the packaging vectors (pMD2.0 G and psPAX) using JetPEI purchased from Qbiogene (Montreal, Quebec, Canada) according to the manufacturer's suggested protocol. The medium was replaced 4 h after transfection, and the cells were cultured for an additional 36 h. Viral particles were harvested, filtered using a 0.45-μm syringe filter, and combined with 8 μg/mL polybrene (Millipore, Boston, MA, USA). PASMCs at 60% confluency were treated with these particles overnight. The culture medium was replaced with fresh complete growth medium, and the cells were cultured for an additional 24 h and then selected with puromycin (8.0 μg/mL) for 36 h. The selected cells were used in the experiments.

Wound healing assay

Human or rat PASMC responses to vascular injury were evaluated in a scratch wound healing assay [15]. The cells were seeded into 6-well plates at a density of 1×10^7/well. When almost fully confluent, the cells were wounded using a standard 1-mL pipette to make a scratch across the diameter of the well. Images were acquired at 0 and 48 h.

Transwell assay

Human PASMCs were digested into a single cell suspension and suspended at 2.5×10^5/mL in serum-free DMEM. A 200-μL cell suspension was added to the transwell upper chamber, and 800 μL DMEM high sugar medium supplemented with 10% FBS was added to the transwell lower chamber. PASMCs were treated with sitagliptin and 1% hypoxic conditions as indicated. Then, those cells in the lower chamber were stained with 1% crystal violet after 15 h and photographed for statistical analysis.

Cytotoxicity assay

PASMCs were seeded into 96-well plates at a density of 3000/well and allowed to adhere in complete medium under normoxic conditions. The cells were treated with 1–1000 μM sitagliptin for 48 h, after which the culture medium was removed. A CCK-8 cell proliferation assay kit (Beyotime Biotechnology, Shanghai, China) was used to evaluate cytotoxicity. A total of 110 μL DMEM containing CCK-8 (CCK8:DMEM(*v*/*v*) = 1:10) was added to each well, and the cells were incubated for 4 h. Finally, cell viability was determined by measuring absorbance at 450 nm using an Epoch Microplate Spectrophotometer (BioTek, Winooski, VT, USA).

Quantitative RT-PCR

The mRNA level of dipeptidyl peptidase-4 (DPP4) in PASMCs was determined by quantitative RT-PCR. Total RNA was extracted from PASMCs using TRIzol reagent (Invitrogen, Life Technologies, Carlsbad, CA, USA) according to the manufacturer's protocol. Reverse transcription was performed using Super-Script™ II reverse transcriptase (Life Technologies). cDNA was amplified and detected using SYBR Premix Ex Taq™ (TaKaRa, Dalian, China). β-Actin was used as an internal loading control. The PCR primers were as follows: 5′-GATCATTGCTCCTCCTGAGC-3′ and 5′-ACTCCTGCTTGCTGATCCAC-3′ for β-actin and 5′-AAGTGGCGTGTTCAAGTGTG-3′ and 5′-TCTTCTGGAGTTGGGAGA CC-3′ for DPP4.

In vitro kinase assay

A total of 1 μg of an inhibitor of NF-κB (IκB) kinase (IKK) α or IKKβ was mixed with active mTOR (0.4 μg/60 μL reaction; Cell Signaling Technology, Danvers, MA, USA) in 10 × kinase buffer containing 10 μM ATP and incubated at 30 °C for 30 min. The reaction was stopped by placing the sample on dry ice. The samples were analyzed by mass spectrometry.

Western blotting

Total lysates of harvested lung tissue and cultured PASMCs were obtained. Lung homogenates were prepared in RIPA lysis buffer (Beyotime Biotechnology, Shanghai, China). The protease inhibitor phenylmethylsulfonyl fluoride (1 mM) was added to the buffer in advance. Equivalent amounts of protein were separated on SDS-polyacrylamide gels and transferred to 0.22-μm nitrocellulose membranes (Millipore). Primary antibodies against phospho-Akt (S473, T308, 1:1000), Akt (1:1000), phospho-mTOR (S2481, 1:1000), p70S6K (1:1000), phospho-p70S6K (T389, 1:1000) and mTOR (1:1000) were purchased from Cell Signaling Technology. Primary antibodies against phospho-NF-κB (S536, 1:1000), NF-κB (1:2000), Raptor (1:1000), IKKα (1:1000), phospho-IKKα/β (S180/181, 1:500), IKKα/β (1:1000), IκBα (1:500), DPP4 (1:500), and β-actin (1:1000) were purchased from Abcam (Cambridge, MA, USA). A primary antibody against phospho-IκBα (S32, 1:500) was purchased from Santa Cruz (Dallas, TX, USA). Membranes were incubated with the primary antibodies overnight at 4 °C and then with secondary antibodies for 1 h at room temperature. Signals were detected using a WesternBright ECL kit (Advansta, Menlo Park, CA, USA).

Luciferase reporter assay

HEK293T cells were co-transfected with an NF-κB luciferase plasmid (Beyotime Biotechnology, Shanghai, China) or a DPP4 luciferase plasmid (Sangon Biotech, Shanghai, China) together with other plasmids according to the manufacturers' protocols and experimental design. After 24 h, luciferase activity was assayed using the Dual-Luciferase Reporter Assay System (Promega, Madison, WI, USA) and a luminometer (Glomax 20/20, Promega). Luciferase activity was normalized to Renilla luciferase activity driven by a constitutively expressed promoter in the phRL vector. Basal promoter activity was measured as the fold change relative to that detected using the basic pGL3 vector alone.

Immunoprecipitation (IP)

Cells were lysed in buffer containing 1% (*v*/*v*) Nonidet P-40, 0.5 mM EGTA, 5 mM sodium orthovanadate, 10% (*v*/*v*) glycerol, 100 μg/mL phenylmethylsulfonyl fluoride, 1 μg/mL leupeptin, 1 μg/mL pepstatin A, 1 μg/mL aprotinin, and 50 mM HEPES, pH 7.5. Thereafter, 1000 μL diluted lysate (1 μg protein/μL) was incubated overnight with 5 μg of an antibody for immunoprecipitation (IP). Immune complexes were captured by adding 60 μL of a 1:1 (*v*/*v*) suspension of protein A:Sepharose 4B beads and rotating the mixture for 2 h at 4 °C. The beads were harvested, and the bound proteins were resolved by SDS-PAGE and analyzed by Western blotting. The primary antibodies used for IP are described in the Western blotting section.

Immunofluorescence staining

Rat small pulmonary artery samples were blocked with 5% donkey serum albumin in 600 μL 1 × phosphate-buffered saline/0.03% Triton X-100 (pH 6.0) in a humidified chamber for 1 h at room temperature and were then immunostained with antibodies as follows: (i) 1:100 anti-Ki-67 raised in rabbit (Servicebio, GB13030–2, Wuhan, China) and 1:200 goat anti-rabbit IgG conjugated to 488 (green color, Servicebio, GB25303, Wuhan, China); (ii) 1:100 anti-α-SMA raised in mouse (Servicebio, GB13044, Wuhan, China) and 1:200 goat anti-mouse IgG conjugated to Cy3 (red color, Servicebio, GB21301, Wuhan, China). Image stacks were captured (×40) at room temperature using laser scanning confocal microscopy (NIKON Clsi Confocal Spectral Imaging System; NIKON Instruments Co., Melville, NY, USA).

Modeling studies

The structures of mTOR and IKKβ were retrieved from the RCSB Protein Data Bank (PDB ID:4JSV [16] and 4KIK [17]). In accordance with previous reports [18–20], the coordinates of IKKα (accession number: O15111.2) were constructed using the MODELER program [21], with IKKβ as the template. The generated model was equilibrated by 100.0 ns MD simulation using the GROMACS4.6.7 program [22] and the Charmm27 force field [23]. As previously recommended [19, 20], the detailed binding profiles between mTOR and IKKα/IKKβ were elucidated using the ZDOCK and RDOCK algorithms [24, 25]. The optimal docked complex was selected and further equilibrated by 100.0 ns MD simulation using the GROMACS4.6.7 program [22] and the Charmm27 force field [23]. These molecular simulations were similar to those performed in previous studies [26, 27]. All structural figures were generated using Discovery studio client [28].

According to the Boltzmann energy distribution approach [29], the probability of each binding pattern was evaluated using the following formula [30, 31]:

$$F(\text{state}) \propto e^{-\frac{\Delta G_{\text{bind}}}{kT}} F(\text{state}) \propto e^{-\frac{\Delta G_{\text{bind}}}{kT}}, \quad (1)$$

where ΔG_{bind}, k, and T are the binding free energy, Boltzmann's constant, and thermodynamic temperature, respectively.

Then, the ratio of the probabilities of two binding processes (Boltzmann factor) was calculated using the following formula:

$$\frac{F(\text{state 2})}{F(\text{state 1})} = e^{\frac{\Delta G_{bind1} - \Delta G_{bind2}}{kT}} \quad (2)$$

Bioinformatic prediction

The JASPAR database (http://jaspar.binf.ku.dk/) was used to predict *DPP4* binding sites to NF-κB. JASPAR CORE Vertebrata was selected after entering the main interface, and the upstream *DPP4* 2000 bp promoter sequence was entered into the input sequence region. NF-κB was entered on the left side, and the SCAN button was clicked to obtain the predicted binding site.

Statistical analysis

Student's *t* test and one-way ANOVA followed by a post hoc test were used for comparisons of different groups. Analyses were performed in SAS version 9.3 (SAS Institute Inc., Cary, NC, USA). All *P* values are nominal and two-sided, and $P \le 0.05$ was considered statistically significant.

RESULTS

Akt/mTOR activation was followed by increased NF-κB phosphorylation in an HPH rat model

Wound healing in pulmonary arteries in HPH is usually a pathogenic process. A wound healing assay measures the combined effect of cell migration and proliferation in PASMCs. We found that compared with normoxia, hypoxia dramatically promoted the wound healing of PASMCs in a time-dependent manner (Fig. 1a), and this effect was prevented by treatment with the mTORC1 inhibitor rapamycin for 48 h in a dose-dependent manner (Fig. 1b). These data indicate that mTORC1 activation is required for the hypoxia-induced abnormal wound healing of PASMCs.

To validate mTOR activation in vivo, we generated a rat model of HPH characterized by abnormal media thickening (Fig. 1c). In this model, Akt/mTOR/p70S6K signaling was increased after 1 or

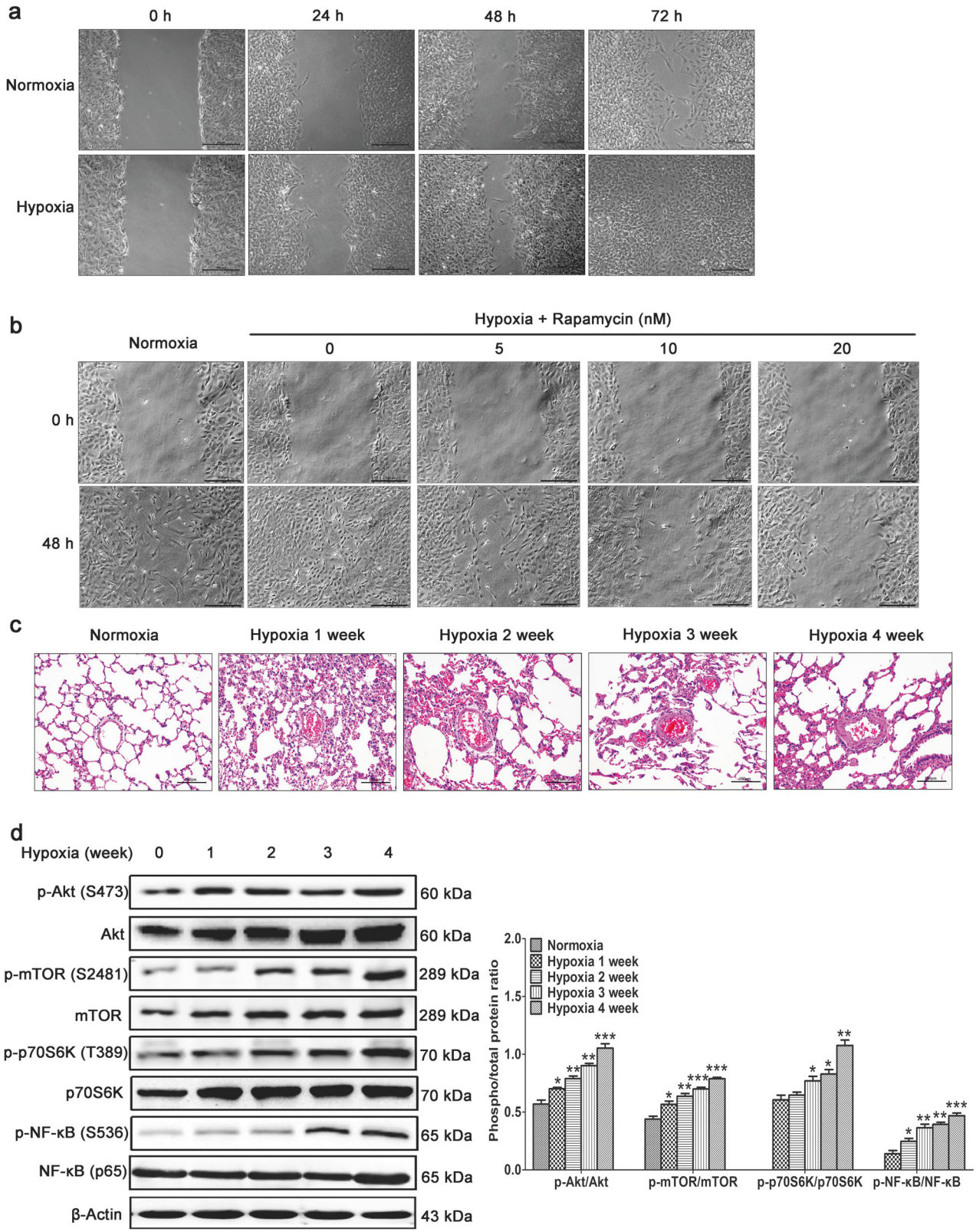

Fig. 1 Akt/mTOR activation was followed by increased NF-κB phosphorylation in the HPH rat model. **a** Primary rat PASMCs were cultured under normoxic or hypoxic conditions. When almost fully confluent, the cells were wounded by scraping, and images were acquired at the different time points as indicated. **b** PASMCs were wounded and stimulated with various concentrations of the mTORC1 inhibitor rapamycin as indicated. For the rat model of HPH, rats ($n = 8$/group) were sacrificed at the different time points as indicated. **c** Hematoxylin-eosin staining of paraffin-fixed lung sections was used for morphological analysis of pulmonary arteries. **d** Western blotting of lung tissue with the indicated antibodies. All the phospho-protein levels were measured by densitometry and normalized to that of total protein. The data are expressed as the means ± standard errors of the means ($n = 8$). *$P < 0.05$, **$P < 0.01$, ***$P < 0.001$

2 weeks of hypoxia stimulation, and the level of phosphorylated NF-κB was subsequently increased at 3 weeks (Fig. 1d). We therefore speculated that mTORC1 might promote hypoxia-induced abnormal responses to vascular injury by increasing NF-κB activity.

Hypoxia-induced mTORC1 activation promotes NF-κB phosphorylation

Hypoxia also activated Akt/mTOR signaling and increased the level of phosphorylated NF-κB in primary cultured PASMCs (Fig. 2a), and this was inhibited by treatment with the PI3K inhibitor LY294002 (Fig. 2b). This demonstrates that the PI3K/Akt/mTOR signaling pathway plays an important role in NF-κB activation. To identify which kinase is responsible for NF-κB phosphorylation, PASMCs cultured under hypoxic conditions were treated with rapamycin. In these cells, mTOR phosphorylation was decreased, as well as phosphorylated NF-κB (Fig. 2c). These findings were confirmed by knockdown of mTOR expression using shRNA (Fig. 2d). To determine whether mTORC1 or mTORC2 increased NF-κB activity, Raptor, a subunit of mTORC1, was knocked down. This dramatically decreased the level of phosphorylated NF-κB. Based on these findings, we conclude that mTORC1 can activate the NF-κB signaling pathway. We next sought to elucidate whether mTORC1 phosphorylates NF-κB or its upstream molecules.

mTORC1 binds to and phosphorylates IKKα and IKKβ

Molecules upstream of the canonical NF-κB signaling pathway include IκBα and IKKα/IKKβ; therefore, molecular docking studies were performed with these molecules and mTOR kinase. Stable binding was detected between mTOR and IKKα/IKKβ separately.

The model generated for IKKα was sufficiently refined by 100 ns MD simulation (Supplementary Fig. S1–S3), consistent with previous MD simulations of IKKβ [32, 33]. The refined IKKα structure is consistent with that of IKKβ, with a backbone-atom root-mean-square deviation (RMSD) of ~2.3 Å (Supplementary Fig. S2).

The mTOR-IKKα and mTOR-IKKβ complexes behaved well during 100 ns MD simulations, oscillating with minor variations and good stereochemical features (Supplementary Fig. S3 and S4). This is consistent with previous multi-timescale dynamic studies of mTOR [34] and IKKβ [32, 33]. Therefore, the equilibrium of these simulations is reliable, and the stable structures are reasonable.

On the basis of our simulation, the PI3K kinase domain (residues 2182–2516) of mTOR can bind directly to the kinase domain (residues 15–302/15–300) of IKKα/IKKβ; however, the binding properties of IKKα and IKKβ with mTOR differ from each other (Fig. 3a). The binding of mTOR with IKKα is characterized by strong hydrogen-bonding interaction networks involving residues Asn2043, Asn2233, Arg2368, Trp2429 and Asp2433 of mTOR and residues Asn28, Leu48, Leu50, Phe181, Asn54, Arg57 and Gln63 of IKKα, with the formation of seven hydrogen bonds (Fig. 3b and Supplementary Table S1). mTOR:Mg^{2+} has electrostatic interactions with the negatively charged pocket containing residues Glu2029 and Glu2033 of mTOR and residues Cys59 and Glu56 of IKKα, with the closest atom distance between mTOR:Mg^{2+} and IKKα:Glu56 being 1.88 Å (Fig. 3b and Supplementary Fig. S5). In the mTOR-IKKα complex, the contact surface areas of mTOR and IKKα are 592.80 and 583.54 $Å^2$, respectively, with polar residues dominating the binding (55.94% and 53.03%, respectively). In the mTOR-IKKβ complex, residues Asp2274, Thr2367, Arg2368, Lys2374, and Asp2517 of mTOR interact with residues Asn225, Arg47, Gly24, and Thr8 of IKKβ, with the formation of only five hydrogen bonds (Fig. 3b and Supplementary Table S2). In contrast with the mTOR-IKKα complex, the contact surface areas of mTOR and IKKβ shrank to ~40% of those in the mTOR-IKKα complex, with values of 355.21 and 363.21 $Å^2$, and it is uncertain which residues dominate the binding. The binding free energies (ΔG_{bind}) of mTOR with IKKα and IKKβ are −23.87 and −14.68 kcal·mol^{-1}, respectively. According to the Boltzmann distribution, mTOR should tend to recruit IKKα rather than IKKβ, with a probability ratio (Boltzmann factor) higher than 245,000.

To confirm the interaction between mTOR and IKKα in primary PASMCs cultured under hypoxic conditions, IP was performed with anti-mTOR and anti-Raptor antibodies. IKKα was detected in both immunoprecipitates by Western blotting (Fig. 3c). Conversely, both mTOR and Raptor were immunoprecipitated by an anti-IKKα antibody (Fig. 3c). To verify the binding of mTORC1 with IKKα, Raptor was knocked down in PASMCs. When IP was performed with an anti-mTOR antibody, IKKα was detected in the immunoprecipitate of PASMCs treated with Mock shRNA (shMock) but not in that of PASMCs treated with Raptor-targeting shRNA (shRaptor) (Fig. 3d), demonstrating that IKKα binds to mTORC1. To confirm the interaction of mTOR with IKKβ, IP was performed with anti-mTOR and anti-Raptor antibodies. IKKβ was detected in both immunoprecipitates by Western blotting. Conversely, both mTOR and Raptor were immunoprecipitated by an anti-IKKβ antibody (Fig. 3e). Accordingly, we conclude that mTORC1 can interact with both IKKα and IKKβ. As a protein kinase, mTOR usually phosphorylates its binding partners. Therefore, we performed in vitro kinase assays using active mTOR and IKKα or IKKβ. Mass spectrometry revealed that mTOR phosphorylated IKKα at Thr23 and phosphorylated IKKβ at Thr559 and Ser634 (Fig. 3f and Supplementary Fig. S6). Accordingly, we speculate that phosphorylation of IKKα and IKKβ by mTOR increases their kinase activities, which could be observed by increased phosphorylation of IKKα/β at Ser180/181 and the downstream protein IκB.

Hypoxia-induced mTORC1 activation enhances the kinase activities of IKKα and IKKβ

To validate the effect of mTORC1 on IKKα and IKKβ, primary cultured PASMCs were exposed to hypoxia. Hypoxia induced mTOR phosphorylation and increased IKKα/β phosphorylation at Ser180/181 (Fig. 4a), and these effects were inhibited by treatment with rapamycin (Fig. 4b) and knockdown of mTOR (Fig. 4c) or Raptor (Fig. 4d). These results indicate that IKKα/β are downstream of and regulated by mTORC1. Activation of the canonical NF-κB signaling pathway was validated in primary PASMCs cultured under hypoxic conditions. Hypoxia induced the phosphorylation of IKKα/β and increased the phosphorylation of the target downstream protein IκBα; then, NF-κB was activated after being released by phospho-IκBα (Fig. 4e). This canonical NF-κB pathway was dramatically inhibited by IKKα/β knockdown in primary PASMCs cultured under hypoxic conditions (Fig. 4f). To validate the effect of mTORC1 on the transcriptional activity of NF-κB, luciferase activity was analyzed in HEK293T cells. Hypoxia dramatically increased NF-κB luciferase activity, and this effect was significantly inhibited by knockdown of mTOR (Fig. 4g) or Raptor (Fig. 4h). We conclude that hypoxia activates mTOR in PASMCs, which enhances the kinase activity of IKKα/β via phosphorylation and thus increases the transcriptional activity of NF-κB. To elucidate the role of NF-κB in HPH, we sought to identify the target proteins and explore their biological function in this condition.

NF-κB promotes DPP4 expression in PASMCs cultured under hypoxic conditions

Bioinformatics demonstrated that the promoter region of *DPP4* contains two NF-κB-binding sites (Supplementary Fig. S7); therefore, this may be a target gene of NF-κB. DPP4 is a glycoprotein of 110 kDa that is ubiquitously expressed on the surface of a variety of cells [35]. This exopeptidase selectively cleaves N-terminal dipeptides from a variety of substrates, including glucagon-like peptide-1 and glucose-dependent insulinotropic polypeptide, which makes it an attractive therapeutic target for type 2 diabetes [36]. Hypoxia increased DPP4 protein expression in PASMCs, and this was inhibited by NF-κB knockdown (Fig. 5a) and increased by

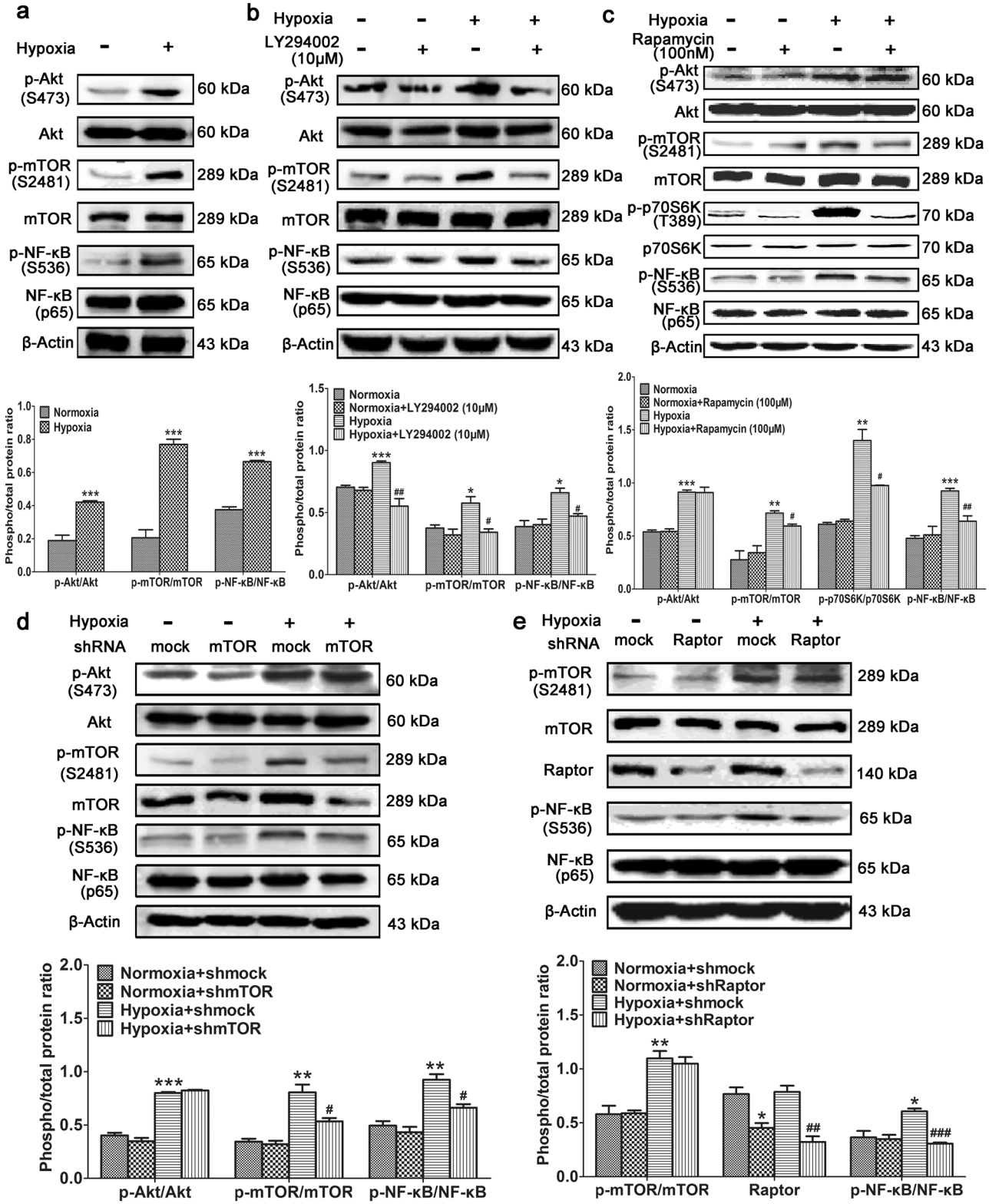

Fig. 2 Hypoxia-induced mTORC1 activation increases NF-κB phosphorylation. Primary PASMCs were (**a**) cultured under hypoxic conditions, (**b**) cultured under hypoxic conditions and treated with the PI3K inhibitor LY294002, or (**c**) cultured under hypoxic conditions and treated with the mTOR inhibitor rapamycin. Western blotting was performed with the indicated antibodies. **d** mTOR or (**e**) Raptor was knocked down in primary PASMCs cultured under hypoxic conditions. Western blotting was performed with the indicated antibodies. All the phospho-protein levels were measured by densitometry and normalized to that of total protein. The data are expressed as the means ± standard errors of the means ($n = 5$). $^{*/\#}P < 0.05$, $^{**/\#\#}P < 0.01$, $^{***/\#\#\#}P < 0.001$

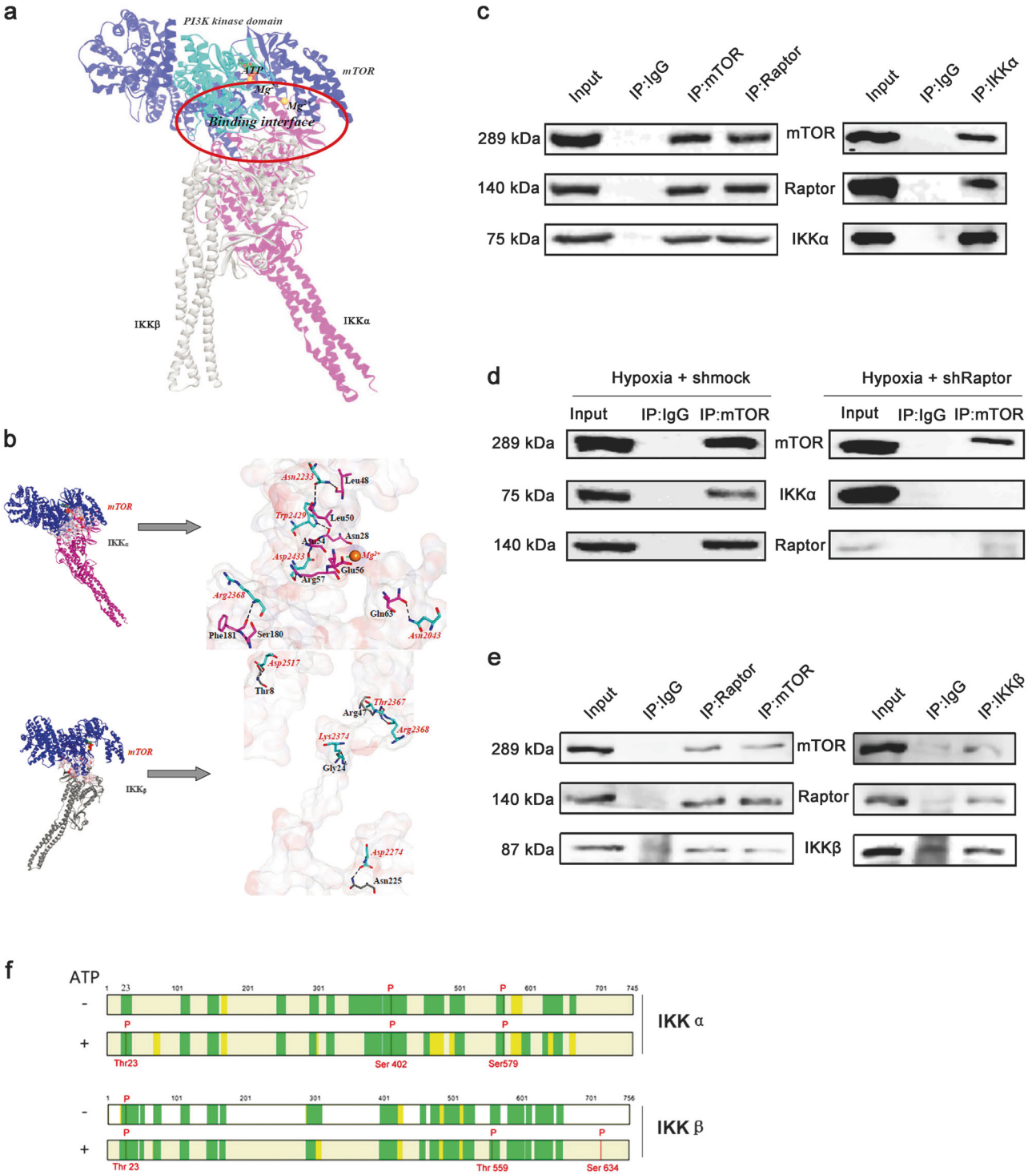

Fig. 3 mTORC1 interacts with and phosphorylates IKKα and IKKβ separately. **a** Superimposition of the binding poses of IKKα and IKKβ with mTOR. IKKα and IKKβ are shown in pink and gray, respectively. mTOR is shown in blue, with its PI3K kinase domain (residues 2182–2516) in cyan. ATP and Mg^{2+} ions are represented by sticks and spheres. **b** Key residues within the binding interfaces of the mTOR-IKKα and mTOR-IKKβ complexes. The Connolly surface of the binding interface was colored according to its electrostatic potential using Discovery Studio scripts. The key residues are shown as sticks. The C atoms are colored cyan, pink, and gray for mTOR, IKKα, and IKKβ, respectively. The H, N, and O atoms are colored white, blue, and red, respectively. The important hydrogen-bonding and electrostatic interactions are shown by dashed black and green lines, respectively. **c** IP with anti-mTOR and anti-Raptor antibodies and immunoblotting with an anti-IKKα antibody (left panel) and IP with an anti-IKKα antibody and immunoblotting with anti-mTOR and anti-Raptor antibodies (right panel) using PASMCs cultured under hypoxic conditions. **d** IP with an anti-mTOR antibody and immunoblotting with an anti-IKKα antibody using PASMCs treated with shMock (left panel) or shRaptor (right panel) and cultured under hypoxic conditions. **e** IP with anti-mTOR and anti-Raptor antibodies and immunoblotting with an anti-IKKβ antibody (left panel) and IP with an anti-IKKβ antibody and immunoblotting with anti-mTOR and anti-Raptor antibodies (right panel) using PASMCs cultured under hypoxic conditions. **f** In vitro kinase assay using active mTOR and IKKα or IKKβ. Mass spectrometry was performed to identify the phosphorylation sites ($n = 5$)

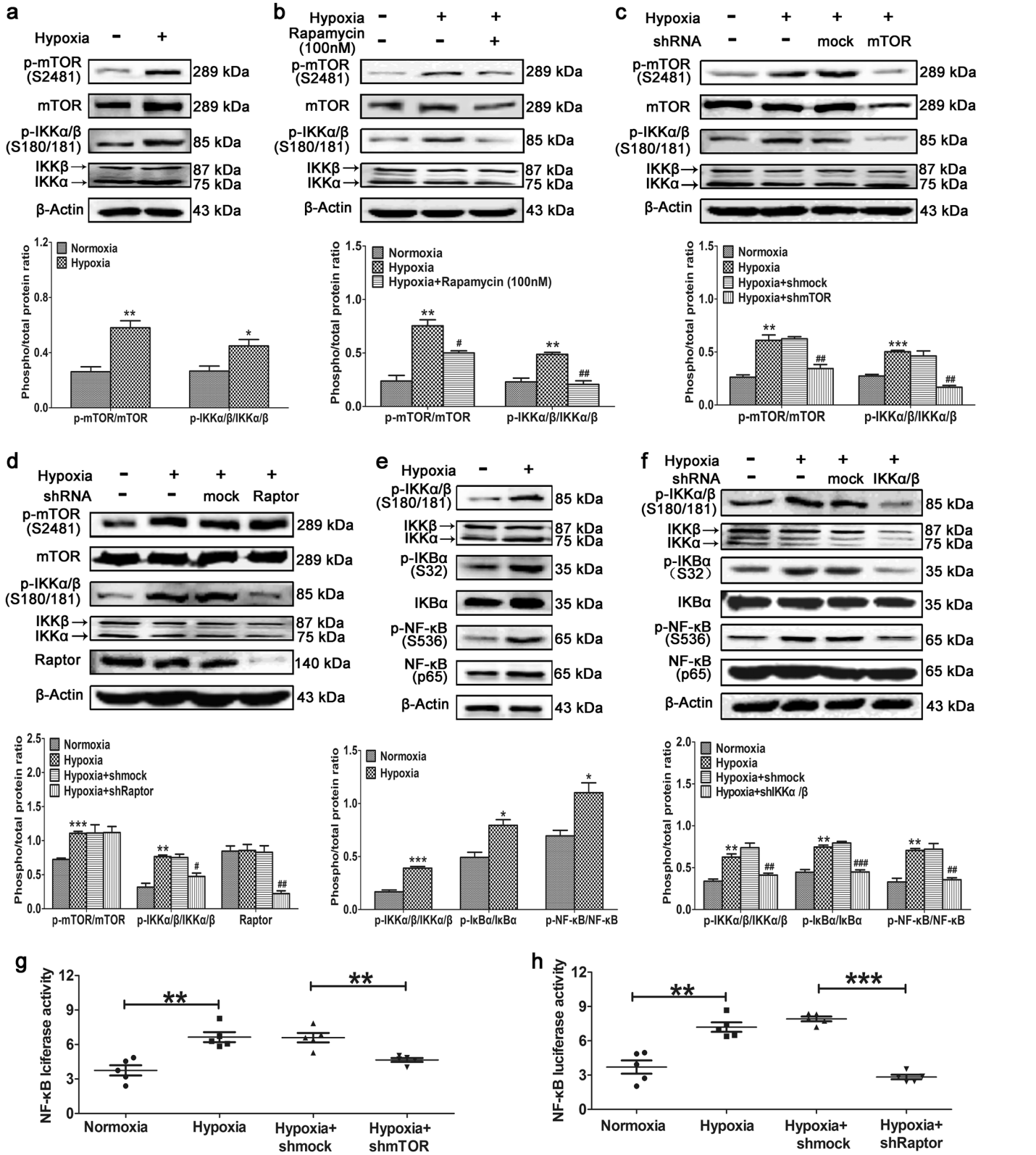

Fig. 4 Hypoxia-induced activation of mTORC1 enhances the kinase activities of IKKα and IKKβ. Primary PASMCs were (**a**) cultured under hypoxic conditions or (**b**) cultured under hypoxic conditions and treated with rapamycin. Western blotting was performed with the indicated antibodies. (**c**) mTOR or (**d**) Raptor was knocked down in primary PASMCs cultured under hypoxic conditions. Western blotting was performed with the indicated antibodies. Primary PASMCs were (**e**) cultured under hypoxic conditions or (**f**) cultured under hypoxic conditions and depleted of IKKα/β. Western blotting was performed with the indicated antibodies. All phospho-protein levels were measured by densitometry and normalized to that of total protein ($n = 5$). HEK293T cells were transfected with the NF-κB luciferase plasmid, cultured under hypoxic conditions, and depleted of (g) mTOR or (**h**) Raptor. NF-κB luciferase activity was analyzed ($n = 5$). The data are expressed as the means ± standard errors of the means. $^{*/\#}P < 0.05$, $^{**/\#\#}P < 0.01$, $^{***/\#\#\#}P < 0.001$

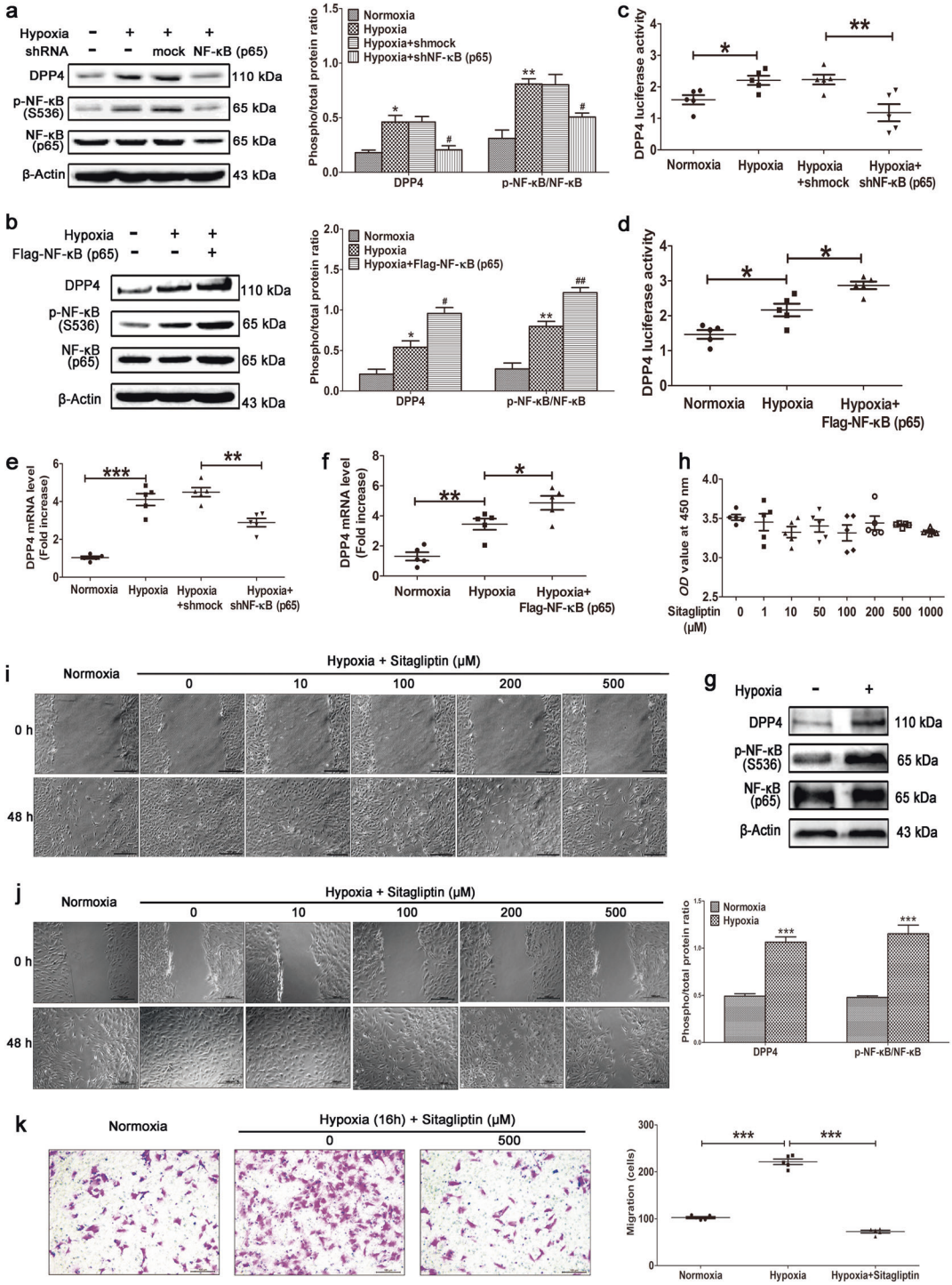

Fig. 5 Hypoxia-induced activation of NF-κB promotes DPP4 expression. NF-κB (p65) was (**a**) knocked down or (**b**) overexpressed in primary PASMCs cultured under hypoxic conditions. Western blotting was performed with the indicated antibodies. All phospho-protein levels were measured by densitometry and normalized to that of total protein ($n = 5$). NF-κB (p65) was (**c**) knocked down or (**d**) overexpressed in HEK293T cells transfected with the DPP4 luciferase plasmid and cultured under hypoxic conditions. DPP4 luciferase activity was analyzed ($n = 5$). NF-κB (p65) was (**e**) knocked down or (**f**) overexpressed in primary PASMCs cultured under hypoxic conditions. Quantitative RT-PCR was performed to examine the mRNA level of *DPP4* ($n = 5$). **g** Primary cultured human PASMCs were stimulated by hypoxia, and Western blotting was performed with the indicated antibodies. phospho-p65 levels were measured by densitometry and normalized to that of total protein ($n = 5$). **h** Cytotoxicity assay using primary cultured PASMCs stimulated with various concentrations of sitagliptin ($n = 5$). Primary rat PASMCs (**i**) and primary human PASMCs (**j**) were cultured under hypoxic conditions. When almost fully confluent, PASMCs were wounded by scraping and treated with the indicated concentration of sitagliptin. Images were acquired at 0 and 48 h ($n = 6$). **k** Human PASMCs were cultured in a transwell upper chamber and stimulated with hypoxia and sitagliptin. The migrated cells in the lower chamber were stained with a 1% crystal violet solution after 15 h and photographed for statistical analysis ($n = 5$). The data are expressed as the means ± standard errors of the mean. $^{*/\#}P < 0.05$, $^{**/\#\#}P < 0.01$, $^{***}P < 0.001$

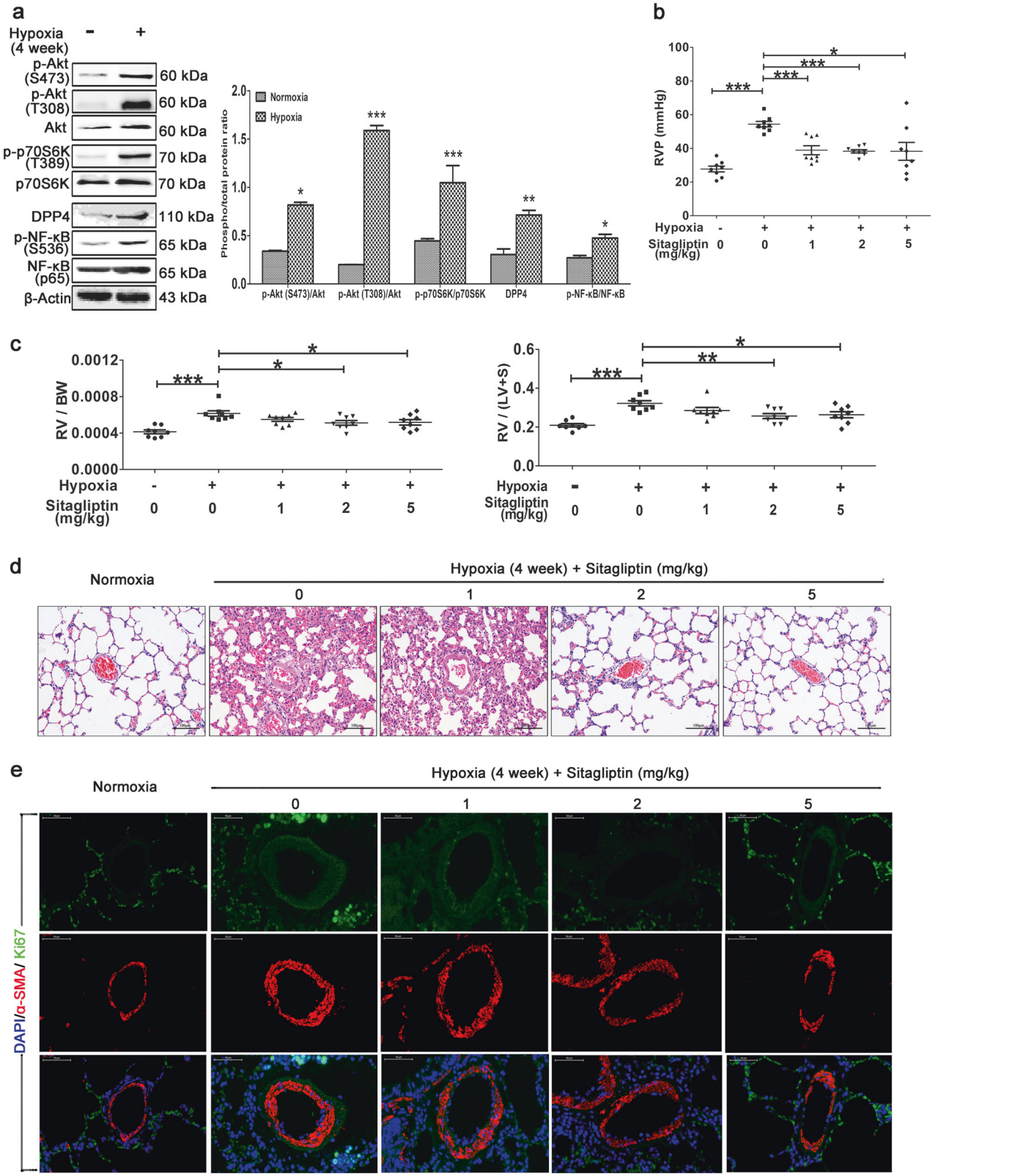

Fig. 6 The DPP4 inhibitor sitagliptin significantly reverses HPH. A rat model of HPH was generated as described previously ($n = 8$/group). The experimental groups were treated with the indicated doses of sitagliptin. **a** Western blotting of lung tissue with the indicated antibodies. All phospho-protein levels were measured by densitometry and normalized to that of total protein. The (**b**) RVP and (**c**) RV/BW and RV/(LV+S) ratios were calculated. The data are expressed as the means ± standard errors of the mean ($n = 8$). *$P < 0.05$, **$P < 0.01$, ***$P < 0.001$. **d** HE staining of paraffin-fixed lung sections for the morphological analysis of pulmonary arteries. **e** Immunofluorescence co-staining of Ki-67 and α-SMA in small pulmonary arteries (40×, $n = 8$)

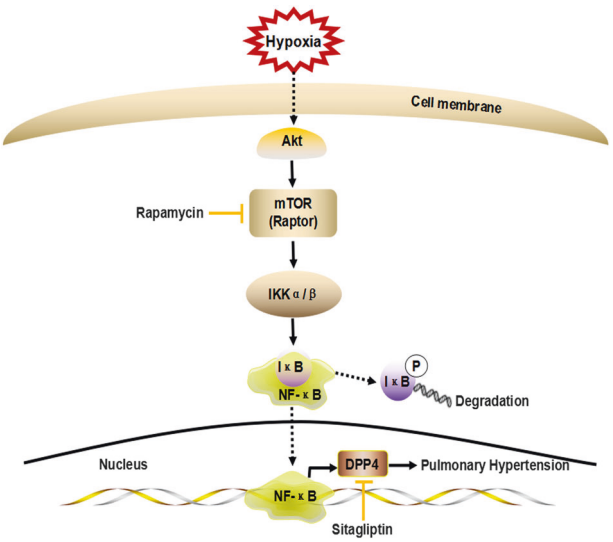

Fig. 7 Schematic diagram of mTORC1/NF-κB/DPP4 signaling pathway activation in HPH. Hypoxia activates the Akt/mTORC1 signaling pathway in PASMCs; mTORC1 phosphorylates IKKα/β, and IKKα/β then phosphorylates IκB. This leads to the degradation of IκB and thus the release and activation of NF-κB. Activated NF-κB moves to the nucleus and induces the expression of its target gene *DPP4*. Inhibition of DPP4 by sitagliptin can attenuate HPH

NF-κB overexpression (p65) (Fig. 5b). A DPP4 luciferase assay indicated that hypoxia dramatically increased *DPP4* transcription, and this was significantly inhibited by NF-κB knockdown (Fig. 5c) and dramatically increased by NF-κB overexpression (Fig. 5d). Quantitative RT-PCR revealed that hypoxia increased *DPP4* mRNA expression in PASMCs, and this was inhibited by NF-κB knockdown (Fig. 5e) and increased by NF-κB overexpression (p65) (Fig. 5f). A Western blot of primary cultured hPASMCs further validated that hypoxia increased the protein expression of DPP4 as well as the phosphorylation level of NF-κB (p65) (Fig. 5g). Sitagliptin is the first approved orally active, potent, selective, and nonpeptidomimetic DPP4 inhibitor [37]. It had no obvious cytotoxic effects on cultured PASMCs, even at a concentration of 1 mM (Fig. 5h). Sitagliptin significantly inhibited the hypoxia-induced abnormal wound healing of rat PASMCs in a dose-dependent manner (Fig. 5i), and the same effects were observed in primary cultured human PASMCs (Fig. 5j). A transwell assay further validated that sitagliptin significantly inhibited human PASMC migration (Fig. 5k). All these findings indicate that hypoxia-induced NF-κB activation promotes DPP4 expression and that inhibition of DPP4 significantly inhibits hypoxia-induced abnormal responses to vascular injury in PASMCs. We speculated that DPP4 might play an important role in HPH and that inhibition of DPP4 might have a beneficial effect on this condition.

Preventive effects of sitagliptin in a rat model of HPH

DPP4 expression in the lung tissue of rats with HPH dramatically increased after 4 weeks of hypoxia, and this was accompanied by increased expression and phosphorylation of NF-κB (Fig. 6a). Sitagliptin significantly decreased RVP (Fig. 6b) and inhibited right ventricular remodeling by decreasing the RV/body weight (BW) (Fig. 6c left) and RV/(LV+S) ratios (Fig. 6c right) compared with exposure to hypoxia and not treatment with this inhibitor. Morphological analysis revealed that sitagliptin significantly attenuated pulmonary artery remodeling by dramatically decreasing the number of smooth muscle cells in the media (Fig. 6d). Immunofluorescence co-staining of Ki-67 and α-SMA revealed that PASMC proliferation in small pulmonary arteries was significantly lower in the sitagliptin group than in the vehicle group (Fig. 6e).

Based on these data, we conclude that hypoxia promotes an abnormal response to vascular injury by activating the Akt/mTORC1 signaling pathway and that mTORC1 enhances NF-κB activity by phosphorylating IKKα/β. Hypoxia-induced NF-κB activation promotes the expression of its target protein DPP4. The DPP4 inhibitor sitagliptin can significantly attenuate pulmonary artery and right heart remodeling and is thus an attractive drug target for HPH (Fig. 7).

DISCUSSION

In HPH, Akt/mTOR signaling pathway activation promotes the proliferation and apoptosis resistance of PASMCs and plays a key role in pulmonary artery remodeling [5, 38]. However, the role of this pathway in the abnormal response to vascular injury is less studied. In this study, we found that hypoxia-induced activation of Akt/mTOR signaling promotes PASMC abnormal wound healing, and this effect is inhibited by the mTORC1 inhibitor rapamycin.

The expression of NF-κB is increased in the lung tissue of a rat model of HPH and in patients with end-stage idiopathic pulmonary arterial hypertension [10, 13]. Inhibition of NF-κB has a therapeutic effect against PH in animal studies [11, 12, 39]. In a rat model of HPH, we found that Akt/mTOR signaling was activated and the level of phosphorylated NF-κB (p65) was subsequently increased, indicating that crosstalk occurs between mTORC1 and NF-κB signaling. An in vitro study of primary PASMCs cultured under hypoxic conditions confirmed that mTORC1 is upstream of NF-κB activation. Investigation of the underlying regulatory mechanism indicated that mTORC1 bound to and phosphorylated both IKKα and IKKβ, which enhanced their kinase activities. IKKα/IKKβ subsequently phosphorylated IκB, inducing the release and thus the activation of NF-κB. This is the first study to find detailed crosstalk between the Akt/mTORC1 and NF-κB signaling pathways.

Hypoxia-induced activation of mTORC1 increased not only the phosphorylation of NF-κB but also its transcriptional activity. As a proinflammatory factor, activation of NF-κB can induce vascular inflammation in endothelial and smooth muscle cells [40]. Blockade of the NF-κB signaling pathway inhibits H_2O_2-induced oxidative stress and inflammation in rat VSMCs [41, 42]. NF-κB is also required for tumor necrosis factor-alpha-directed [43] and IL-18-induced [44] smooth muscle cell migration. To explore new potential treatment options for HPH, it is crucial to study target proteins of NF-κB and the effects of their inhibitors on the abnormal wound healing of primary PASMCs cultured under hypoxic conditions. We found that DPP4 is a target protein of NF-κB activated under hypoxia and that DPP4 inhibition significantly inhibited the abnormal response to vascular injury of PASMCs and attenuated pulmonary artery and right heart remodeling in a rat model of HPH. These data imply that DPP4 inhibition might have beneficial effects against HPH.

Left-sided hemodynamics are critical for any PH study because off-target effects of interventions can affect systemic physiology, which is not consistent with human PAH. There were limitations to the rat hypoxia-induced PH model because we did not check the left heart hemodynamics or quantify sitagliptin uptake. Another limitation is that primary cultured human or rat PASMCs were verified only by staining for smooth muscle α-actin at each passage, which was not sufficient for confirming PASMC lineage.

In conclusion, hypoxia can induce an abnormal response to vascular injury by activating the Akt/mTORC1 signaling pathway. Crosstalk between the Akt/mTORC1 and NF-κB signaling pathways via phosphorylation of IKKα/β by mTORC1 increases the transcriptional activity of NF-κB. DPP4 is a target protein of NF-κB in hypoxia-induced abnormal responses to vascular injury. The DPP4 inhibitor sitagliptin significantly attenuates pulmonary artery and right heart remodeling, and DPP4 is thus an attractive drug target for HPH.

ACKNOWLEDGEMENTS

This work was supported by the National Natural Science Foundation of China (Nos. 81670045, 81272586, and 81470249) and the Chinese Postdoctoral Science Foundation (No. 2014M560759).

AUTHOR CONTRIBUTIONS

SQL designed the experiments and prepared the initial manuscript. YL and LY conducted the experiments. LD, JZ and NZ cultivated the cells. ZWY and SLZ were responsible for the experimental calculations. JWX, YG, MJN, XJZ, YYZ, XMW, YZZ and PZ were involved in the experimental analysis. YL, LY, LD, ZWY and JZ contributed equally to this manuscript. SQL is the corresponding author.

ADDITIONAL INFORMATION

The online version of this article (https://doi.org/10.1038/s41401-019-0272-2) contains supplementary material, which is available to authorized users.

Competing interests: The authors declare no competing interests.

REFERENCES

1. Pugliese SC, Poth JM, Fini MA, Olschewski A, El Kasmi KC, Stenmark KR. The role of inflammation in hypoxic pulmonary hypertension: from cellular mechanisms to clinical phenotypes. Am J Physiol Lung Cell Mol Physiol. 2015;308:L229–52.
2. Voelkel NF, Tamosiuniene R, Nicolls MR. Challenges and opportunities in treating inflammation associated with pulmonary hypertension. Expert Rev Cardiovasc Ther. 2016;14:939–51.
3. Paulin R, Meloche J, Courboulin A, Lambert C, Haromy A, Courchesne A, et al. Targeting cell motility in pulmonary arterial hypertension. Eur Respir J. 2014;43:531–44.
4. Wang AP, Li XH, Yang YM, Li WQ, Zhang W, Hu CP, et al. A critical role of the mTOR/eIF2alpha pathway in hypoxia-induced pulmonary hypertension. PLoS ONE. 2015;10:e0130806.
5. Ma X, Yao J, Yue Y, Du S, Qin H, Hou J, et al. Rapamycin reduced pulmonary vascular remodelling by inhibiting cell proliferation via Akt/mTOR signalling pathway down-regulation in the carotid artery-jugular vein shunt pulmonary hypertension rat model. Interact Cardiovasc Thorac Surg. 2017;25:206–11.
6. Houssaini A, Abid S, Mouraret N, Wan F, Rideau D, Saker M, et al. Rapamycin reverses pulmonary artery smooth muscle cell proliferation in pulmonary hypertension. Am J Respir Cell Mol Biol. 2013;48:568–77.
7. Kudryashova TV, Goncharov DA, Pena A, Ihida-Stansbury K, DeLisser H, Kawut SM, et al. Profiling the role of mammalian target of rapamycin in the vascular smooth muscle metabolome in pulmonary arterial hypertension. Pulm Circ. 2015;5:667–80.
8. Ruygrok PN, Muller DW, Serruys PW. Rapamycin in cardiovascular medicine. Intern Med J. 2003;33:103–9.
9. Bee J, Fuller S, Miller S, Johnson SR. Lung function response and side effects to rapamycin for lymphangioleiomyomatosis: a prospective national cohort study. Thorax. 2018;73:369–75.
10. Fan J, Fan X, Li Y, Ding L, Zheng Q, Guo J, et al. Chronic normobaric hypoxia induces pulmonary hypertension in rats: role of NF-kappaB. High Alt Med Biol. 2016;17:43–9.
11. Farkas D, Alhussaini AA, Kraskauskas D, Kraskauskiene V, Cool CD, Nicolls MR, et al. Nuclear factor kappaB inhibition reduces lung vascular lumen obliteration in severe pulmonary hypertension in rats. Am J Respir Cell Mol Biol. 2014;51:413–25.
12. Zhu R, Bi L, Kong H, Xie W, Hong Y, Wang H. Ruscogenin exerts beneficial effects on monocrotaline-induced pulmonary hypertension by inhibiting NF-kappaB expression. Int J Clin Exp Pathol. 2015;8:12169–76.
13. Price LC, Caramori G, Perros F, Meng C, Gambaryan N, Dorfmuller P, et al. Nuclear factor kappa-B is activated in the pulmonary vessels of patients with end-stage idiopathic pulmonary arterial hypertension. PLoS ONE. 2013;8:e75415.
14. Luo Y, Xu DQ, Dong HY, Zhang B, Liu Y, Niu W, et al. Tanshinone IIA inhibits hypoxia-induced pulmonary artery smooth muscle cell proliferation via Akt/Skp2/p27-associated pathway. PLoS ONE. 2013;8:e56774.
15. Deng L, Blanco FJ, Stevens H, Lu R, Caudrillier A, McBride M, et al. MicroRNA-143 activation regulates smooth muscle and endothelial cell crosstalk in pulmonary arterial hypertension. Circ Res. 2015;117:870–83.
16. Yang H, Rudge DG, Koos JD, Vaidialingam B, Yang HJ, Pavletich NP. mTOR kinase structure, mechanism and regulation. Nature. 2013;497:217–23.
17. Liu S, Misquitta YR, Olland A, Johnson MA, Kelleher KS, Kriz R, et al. Crystal structure of a human IkappaB kinase beta asymmetric dimer. J Biol Chem. 2013;288:22758–67.
18. Moss BL, Gross S, Gammon ST, Vinjamoori A, Piwnica-Worms D. Identification of a ligand-induced transient refractory period in nuclear factor-kappaB signaling. J Biol Chem. 2008;283:8687–98.
19. Li Y, Yang Z, Li W, Xu S, Wang T, Wang T, et al. TOPK promotes lung cancer resistance to EGFR tyrosine kinase inhibitors by phosphorylating and activating c-Jun. Oncotarget. 2016;7:6748–64.
20. Xu S, Wang T, Yang Z, Li Y, Li W, Wang T, et al. miR-26a desensitizes non-small cell lung cancer cells to tyrosine kinase inhibitors by targeting PTPN13. Oncotarget. 2016. https://doi.org/10.18632/oncotarget.9920.
21. Webb B, Sali A. Comparative protein structure modeling using MODELLER. Curr Protoc Bioinforma / Ed board. 2014;47:5.6.1–5.6.32.
22. Pronk S, Pall S, Schulz R, Larsson P, Bjelkmar P, Apostolov R, et al. GROMACS 4.5: a high-throughput and highly parallel open source molecular simulation toolkit. Bioinformatics. 2013;29:845–54.
23. Brooks BR, Brooks CL 3rd, Mackerell AD Jr, Nilsson L, Petrella RJ, Roux B, et al. CHARMM: the biomolecular simulation program. J Comput Chem. 2009;30:1545–614.
24. Chen R, Li L, Weng Z. ZDOCK: an initial-stage protein-docking algorithm. Proteins. 2003;52:80–7.
25. Li L, Chen R, Weng Z. RDOCK: refinement of rigid-body protein docking predictions. Proteins. 2003;53:693–707.
26. Yang Z, Yang G, Zhou L. Mutation effects of neuraminidases and their docking with ligands: a molecular dynamics and free energy calculation study. J Comput Aided Mol Des. 2013;27:935–50.
27. Yang Z, Wu F, Yuan X, Zhang L, Zhang S. Novel binding patterns between ganoderic acids and neuraminidase: Insights from docking, molecular dynamics and MM/PBSA studies. J Mol Graph Model. 2016;65:27–34.
28. Accelrys. Discovery Studio 3.1. 2011. http://accelrys.com. Accessed 25 Jul 2013.
29. Park J-W, Kim CU, Isard W. Permit allocation in emissions trading using the Boltzmann distribution. Phys A. 2012;391:4883–90.
30. Krymskaya VP, Snow J, Cesarone G, Khavin I, Goncharov DA, Lim PN, et al. mTOR is required for pulmonary arterial vascular smooth muscle cell proliferation under chronic hypoxia. FASEB J. 2011;25:1922–33.
31. Samokhin AO, Stephens T, Wertheim BM, Wang RS, Vargas SO, Yung LM, et al. NEDD9 targets COL3A1 to promote endothelial fibrosis and pulmonary arterial hypertension. Sci Transl Med. 2018;10:eaap7294.
32. Jones MR, Liu C, Wilson AK. Molecular dynamics studies of the protein-protein interactions in inhibitor of kappaB kinase-beta. J Chem Inf Model. 2014;54:562–72.
33. Park H, Shin Y, Choe H, Hong S. Computational design and discovery of nanomolar inhibitors of IkappaB kinase beta. J Am Chem Soc. 2015;137:337–48.
34. Sapienza PJ, Mauldin RV, Lee AL. Multi-timescale dynamics study of FKBP12 along the rapamycin-mTOR binding coordinate. J Mol Biol. 2011;405:378–94.
35. Ghate M, Jain SV. Structure based lead optimization approach in discovery of selective DPP4 inhibitors. Mini Rev Med Chem. 2013;13:888–914.
36. Rohrborn D, Wronkowitz N, Eckel J. DPP4 in diabetes. Front Immunol. 2015;6:386.
37. Suresh PS, Srinivas NR, Mullangi R. A concise review of the bioanalytical methods for the quantitation of sitagliptin, an important dipeptidyl peptidase-4 (DPP4) inhibitor, utilized for the characterization of the drug. Biomed Chromatogr. 2016;30:749–71.
38. Aghamohammadzadeh R, Zhang YY, Stephens TE, Arons E, Zaman P, Polach KJ, et al. Up-regulation of the mammalian target of rapamycin complex 1 subunit Raptor by aldosterone induces abnormal pulmonary artery smooth muscle cell survival patterns to promote pulmonary arterial hypertension. FASEB J. 2016;30:2511–27.
39. Liu ZQ, Liu B, Yu L, Wang XQ, Wang J, Liu HM. Simvastatin has beneficial effect on pulmonary artery hypertension by inhibiting NF-kappaB expression. Mol Cell Biochem. 2011;354:77–82.
40. Liu M, Yu P, Jiang H, Yang X, Zhao J, Zou Y, et al. The essential role of Pin1 via NF-kappaB signaling in vascular inflammation and atherosclerosis in ApoE$^{-/-}$ Mice. Int J Mol Sci. 2017;18:E644.
41. Huang M, Zeng S, Zou Y, Shi M, Qiu Q, Xiao Y, et al. The suppression of bromodomain and extra-terminal domain inhibits vascular inflammation by blocking NF-kappaB and MAPK activation. Br J Pharmacol. 2017;174:101–15.
42. Wang YL, Sun GY, Zhang Y, He JJ, Zheng S, Lin JN. Tormentic acid inhibits H2O2-induced oxidative stress and inflammation in rat vascular smooth muscle cells via inhibition of the NF-kappaB signaling pathway. Mol Med Rep. 2016;14:3559–64.
43. Wang Z, Castresana MR, Newman WH. NF-kappaB is required for TNF-alpha-directed smooth muscle cell migration. FEBS Lett. 2001;508:360–4.
44. Chandrasekar B, Mummidi S, Mahimainathan L, Patel DN, Bailey SR, Imam SZ, et al. Interleukin-18-induced human coronary artery smooth muscle cell migration is dependent on NF-kappaB- and AP-1-mediated matrix metalloproteinase-9 expression and is inhibited by atorvastatin. J Biol Chem. 2006;281:15099–109.